Geophysical Research Letters

Supporting Information for

Controls on stable water isotopes in monsoonal precipitation across the Bay of Bengal: atmosphere and surface analysis

Jingyi Zhang[1], Wusheng Yu[1], Stephen Lewis[2], Lonnie G. Thompson[3], Gabriel J. Bowen[4], Kei Yoshimura[5,6], Alexandre Cauquoin[5], Martin Werner[7], Supriyo Chakraborty[8,9], Zhaowei Jing[10], Yaoming Ma[1], Xiaoyu Guo[1], Baiqing Xu[1], Guangjian Wu[1], Rong Guo[1,11], Dongmei Qu[1]

[1]State Key Laboratory of Tibetan Plateau Earth System, Environment and Resources (TPESER), Institute of Tibetan Plateau Research, Chinese Academy of Sciences, Beijing 100101, China

[2]Catchment to Reef Research Group, Centre for Tropical Water and Aquatic Ecosystem Research, James Cook University, Townsville, QLD 4811, Australia

[3]Byrd Polar and Climate Research Center, The Ohio State University, Columbus, OH 43210, USA

[4]Department of Geology and Geophysics, University of Utah, Salt Lake City, UT84112, USA

[5]Institute of Industrial Science, The University of Tokyo, Kashiwa, Japan

[6]Earth Observation Research Center, Japan Aerospace Exploration Agency, Japan

[7]Alfred Wegener Institute (AWI), Helmholtz Centre for Polar and Marine Sciences, Bremerhaven, Germany

[8]Indian Institute of Tropical Meteorology, Ministry of Earth Sciences, Pune, India

[9]Department of Atmospheric and Space Sciences, Savitribai Phule Pune University, Pune, India

[10]Function Laboratory for Ocean Dynamics and Climate, Pilot National Laboratory for Marine Science and Technology (QNLM), Qingdao, 266237, China

[11]University of Chinese Academy of Sciences, Beijing 100049, China

Corresponding author: W. Yu (yuws@itpcas.ac.cn)

Contents of this file

Text S1 Description for the three study sites

The three study sites of Port Blair, Barisal, and Darjeeling were selected in this study. Port Blair (16 m a.s.l.) is located on the Andaman and Nicobar Islands, which sit to the southeast of the BoB (Figure 1a). Barisal is a port city in southern Bangladesh and is located on the coastal plain at the head of the BoB (Figure 1a) with an altitude of 7 m a.s.l. (Table S1). Darjeeling, in West Bengal, India, is the most northern site in our study area (Figure 1a). The site sits on the Sivalik Mountains in the southern foothills of the Himalayas and has a relatively high altitude (2042 m a.s.l.) (Figure 1a and Table S1). During the monsoon season (May–September), all three sites are influenced by the Indian Summer Monsoon (ISM) (Figure 1a) and receive abundant precipitation which accounts for more than 80% of their respective total annual precipitation.

Text S2 Precipitation and water vapor stable isotope data

The observed stable hydrogen isotopes in daily precipitation (δD_p) from Port Blair during 2012–2016 and Barisal during 2013–2015 were from the International Atomic Energy Agency's (IAEA) coordinated Research Project (CRP) F31004 (Munksgaard et al., 2019). The daily δD_p data from Darjeeling during 2013–2018 were observed by Chakraborty et al. (2022), but released in this study. The detailed sampling and measurement procedures were published by Chakraborty et al. (2022).

As δD_p records properties inherent within the upstream water vapor sources and transport processes, it is instructive to examine the characteristics of the upstream stable hydrogen isotopes in water vapor (δD_v). The δD_v from different vertical atmospheric levels were retrieved from the Tropospheric Emission Spectrometer (TES) onboard NASA's Earth Observing System Aura satellite. TES is an infrared high-resolution Fourier transform spectrometer (FTS) that measures the spectral infrared (IR) radiances in 650–3050 cm^{-1} with an apodized spectral resolution of ~0.1 cm^{-1} (Worden et al., 2006; 2012). TES can complete one global survey every 2 days with a combined horizontal footprint of 5.3 by 8.4 km in the nadir viewing mode (Worden et al., 2004, 2006, 2012). TES measures the HDO/H_2O ratio at 17 pressure levels and are sensitive between the surface (1000 hPa) and about 300 hPa with a peak sensitivity at 700 hPa in the low latitudes (Worden et al., 2006). As the accuracy of the retrieved δD_v is related to temperature and water amount, the sensitivity decreases with latitude (Worden et al., 2006). Consequently, the retrieved δD_v has the least uncertainty in the tropics and higher uncertainties at the higher latitudes (Worden et al., 2006). In this study, we used the TES Level 2 lite product (version 7), and the bias has been accounted for and incorporated in the version 7 product (Pradhan et al., 2019; Worden et al., 2011). The data were filtered using the quality control criteria with degrees of freedom less than 1.5 and a retrieved quality of 0. The average cloud optical depth is less than 0.4 (Worden et al., 2012). We extracted the δD_v data from 1000 to 510 hPa (moisture transport mainly occurs in middle- and lower-troposphere) for the years 2006 to 2009 (the effective years of the retrieved δD_v) to calculate the multi-monthly δD_v variability (May–September). Indeed, the time period of the TES data is different from those of the observed δD_p. However, in this study, we come to the conclusions by calculating the multi-monthly average over 4 years and emphasize this mean state over several years, but not the inter-annual δD_v changes. Therefore, the different time periods do not affect our conclusions.

We also used isotope outputs from two isotope-enabled AGCMs: ECHAM6-wiso (Cauquoin et al., 2019; Cauquoin and Werner, 2021) and IsoGSM2 (Yoshimura et al., 2008).

ECHAM6 is the sixth generation of the general atmospheric circulation model ECHAM (Stevens et al., 2013). The implementation of stable water isotopes in ECHAM6 and its evaluation against various observations have been described in detail by Cauquoin et al. (2019), and this model version has been labeled ECHAM6-wiso. The model has been performed at a relatively high spatial resolution (approx. 0.9° × 0.9° and 95 vertical levels) and with a temporal resolution of 6 h. The fields of temperature, vorticity and divergence as well as the surface pressure field were nudged toward the ERA5 reanalysis data (Hersbach et al., 2020) every 6 hours (see details in Cauquoin and Werner (2021)). Thanks to its high spatial resolution, ECHAM6-wiso improved the topography with improved modeled isotopic composition of precipitation and water vapor over elevated areas like the Himalayas and the Andes. In this study, we used the modeled δD_p and δD_v outputs over the pressure from 1000 to 500 hPa for the same period as the observed δD_p data at each study site.

The simulation from the Isotopes-incorporated Global Spectral Model (IsoGSM2) has been performed at a spatial resolution of 1.9° latitude × 1.8° longitude with 28 atmosphere vertical levels, a temporal resolution of 6 h (Yoshimura et al., 2008). The temperature and zonal and meridional wind components from NCEP/DOE Reanalysis 2 were used to constrain the model using the spectral nudging technique (Yoshimura et al., 2008). In a similar way than ECHAM6-wiso, we used the modeled IsoGSM2 δD_p and δD_v data from the 1000 to 500 hPa levels over the corresponding period of the observed δD_p data for each study site.

Through verification, the modeled δD_p data from ECHAM6-wiso and IsoGSM2 have fairly good agreement with the observed δD_p data at the three study sites (Figure S1). The modeled δD_v from ECHAM6-wiso and IsoGSM2 are also significantly correlated to the δD_v from TES (Figures S2). Therefore, the modeled δD_p and δD_v data from ECHAM6-wiso and IsoGSM2 are well suited to reflect the spatiotemporal patterns of δD_p and δD_v across the study area. In addition, the evaluation of the IsoGSM2 isotopic results against observed stable isotopes in the Indian subcontinent showed that IsoGSM2 is able to capture the temporal and spatial variations of stable isotopes in this region (Midhun & Ramesh, 2016; Midhun et al., 2018; Nimya et al., 2022). Indeed, Nimya et al. (2022) have shown that IsoGSM2 captures the temporal variation of δD_p even in north India (including the elevated locations), near the Himalayas. Those also indicate that IsoGSM2 can fairly reproduce the spatiotemporal patterns of δD_p and δD_v in South Asia.

The modeled δD_v data are relatively lower than the TES-δD_v data at the Port Blair site (Figure S2). In addition, we found that the modeled δD_p data at the Port Blair site are also relatively lower than the observed δD_p. The representation of the tropical region is challenging for climate models. Our model-data disagreements could be due to biases in the representation of the cloudiness (especially the low level clouds) and the convection, as well as biases in the partitioning of precipitation between land and sea (Stevens et al., 2013).

In addition, we compared the modeled δD_p and δD_v of ECHAM6-wiso and the ones of IsoGSM2 at the three study sites. While some differences can be found in the seasonal mean amplitudes between the two models, the results show that the modeled δD_p and δD_v variations from ECHAM6-wiso are similar to those from IsoGSM2 at each site of interest (Figures S3 and S4).

We compared the decreasing trends of upstream δD_v retrieved from TES with those modeled by ECHAM6-wiso and IsoGSM2 during the common time period (2006–2009), and found that the results are similar (Figures S5a, c). Those demonstrate that the different time periods only lead to a slight difference in the amplitude of the decreasing trends in the upstream δD_v, but do not affect the patterns of upstream δD_v. In addition, we found that the decreasing trends of upstream δD_v modeled by ECHAM6-wiso and IsoGSM2 also occurred during a 40-year period (1979–2018) (Figures S5b, d). These results further prove that the patterns of upstream δD_v in our study area are a common phenomenon regardless the considered time period. Therefore, the different time periods between the TES data and other data used in this study do not affect our conclusions.

Text S3 Meteorological data

The daily gridded precipitation amount data, obtained from the NASA's Tropical Rainfall Measuring Mission (TRMM) Multi-Satellite Precipitation Analysis (3B42) Version 7 data (0.25° × 0.25°), were used to determine the correlation between δD_p and upstream accumulative precipitation. We used the outgoing longwave radiation (OLR) data (1° × 1°), obtained from the UMD OLR Climate Data Record (CDR) Portal, to examine the influence of changes in upstream accumulative convection on δD_p. The vertical velocity data (0.25° × 0.25°) covering the 1959–2022 period (64 years) based on ERA5 reanalysis were also used to explore the vertical air motions and their effect on δD_p.

Text S4 Moisture source diagnostic method

The Hybrid Single Particle Lagrangian Integrated Trajectory (HYSPLIT) model version 4.0 was used to identify the air mass back trajectories with the ERA-Interim data at 37 pressure levels (1° × 1° resolution) provided by the European Centre for Medium-Range Weather Forecasts (ECWMF, 1979−2019). We only calculated the back trajectories for precipitation-producing days with time periods of 240-hours at six-hourly intervals. To reduce the uncertainty of a single atmospheric level, trajectories were tracked at 500, 1000, 1500, 2000, 3000, 4000, and 5000 m a.s.l. (Breitenbach et al., 2010; Cai & Tian, 2020). The changes in specific humidity along the back trajectories were calculated to account for the uptake and loss of moisture during the transport process (Sodemann et al., 2008). The spatial patterns of the total upstream moisture contribution areas were quantified using the sum of the specific humidity changes across all grid points.

Text S5 Recognition about the influence of upstream accumulative convection over the initial four days on the downstream δD_p

We calculated the correlations between the observed daily δD_p at the three downstream study sites and the upstream accumulative precipitation amount and upstream average OLR along the back trajectories over the time constant τ_m (10, 9, …, 1, and 0 day prior to the precipitation event), respectively (Figures S11a and S11b). As shown in Figure S11a, the daily δD_p at each downstream site is strongly and negatively correlated with the upstream accumulative precipitation amount along the back trajectories. The negative correlation coefficients for Port Blair increase significantly from $\tau_m = 0$ to $\tau_m = 1$ (r changes from −0.32 to −0.44), then stabilize when $\tau_m > 1$ (from −0.43 to −0.47) (Figure S11a). For Barisal and Darjeeling, the negative correlations show considerable improvement over the time constants until $\tau_m = 4$ (r changes from −0.29 to −0.53 and from −0.16 to −0.22, respectively) (Figure S11a). However, the significance of these negative correlations is slightly improved (r changes from −0.54 to −0.58) at Barisal and gradually becomes weaker at Darjeeling (r changes from −0.21 to −0.02) after four days (Figure S11a). Therefore, the upstream accumulative convection over the initial four days plays a considerable role in governing the changes of downstream δD_p at Barisal and Darjeeling. In addition, the significant increase in positive correlation coefficients between the daily δD_p at the three downstream study sites and the average OLR along the back trajectories over the τ_m also appear in the initial four days (Figure S11b). Moreover, both higher precipitation amount (> 3 mm/day) and lower OLR values (< 240 W/m^2; indicating strong convection) along the back trajectories mainly occur over the initial four days for each downstream site (Figure S11c and S11d). These results prove that the influence of upstream accumulative convection on the downstream δD_p mainly occurs over the initial four days.

Table S1. Summary of the three study sites listed by latitude from south to north.

	Port Blair	Barisal	Darjeeling
Latitude (°N)	11.66	22.72	27.04
Longitude (°E)	92.73	90.35	88.26
Elevation (m a.s.l.)	16	7	2042
Sampling period	2012.5–2016.9	2013.5–2015.9	2013.5–2018.9
Number of samples	443	195	286

Table S2. Summary of the other sites used in this study listed by latitude from south to north.

	Colombo	Hyderabad	Mumbai	Tezpur
Latitude (°N)	6.91	17.45	18.90	26.63
Longitude (°E)	79.87	78.47	72.82	92.80
Elevation (m a.s.l.)	7	545	10	48
Dating period	1983.5–1994.7	1997.9–2000.9	1961.6–1977.9	2015.5–2018.9
Time scale	Monthly	Monthly	Monthly	Daily
Number of samples	30	16	41	201
Data Sources	GNIP	GNIP	GNIP	This study

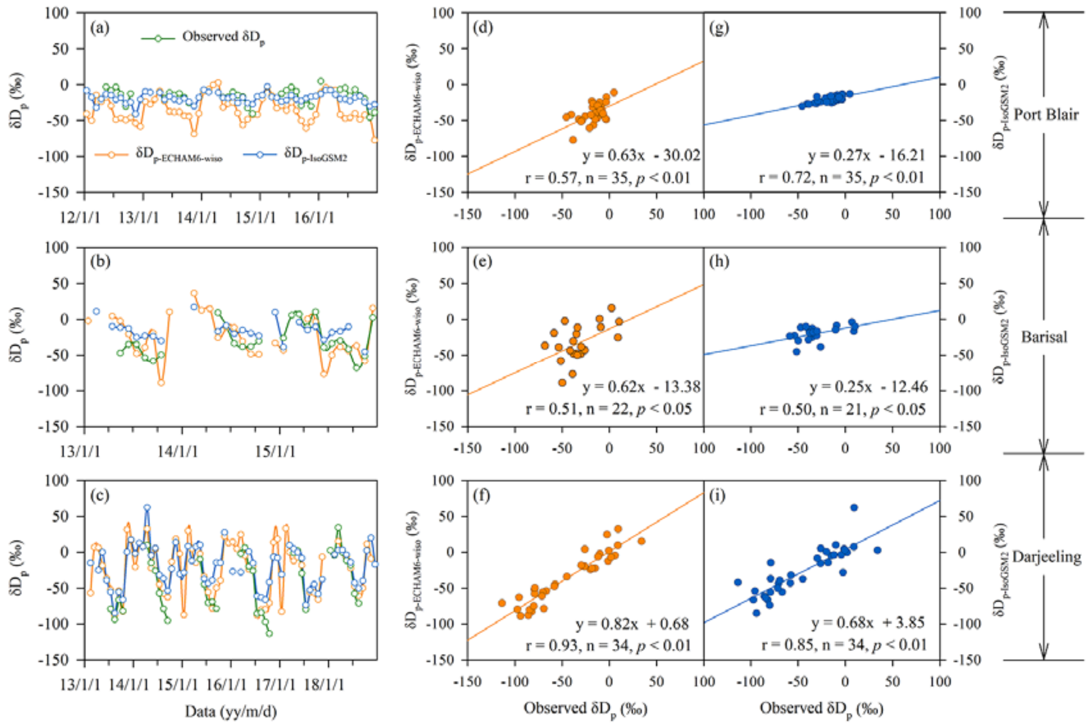

Figure S1. (a–c) Comparisons of observed monthly δD_p (green lines with dots) with the modeled results from ECHAM6-wiso and IsoGSM2 (orange and blue lines with dots, respectively) at Port Blair (a), Barisal (b), and Darjeeling (c). (d–f) The relationships between the observed monthly δD_p and the ECHAM6-wiso modeled monthly δD_p at Port Blair (d), Barisal (e), and Darjeeling (f). (g–i) The same plots as (d–f) but for the relationships between the observed monthly δD_p and the IsoGSM2 modeled monthly δD_p.

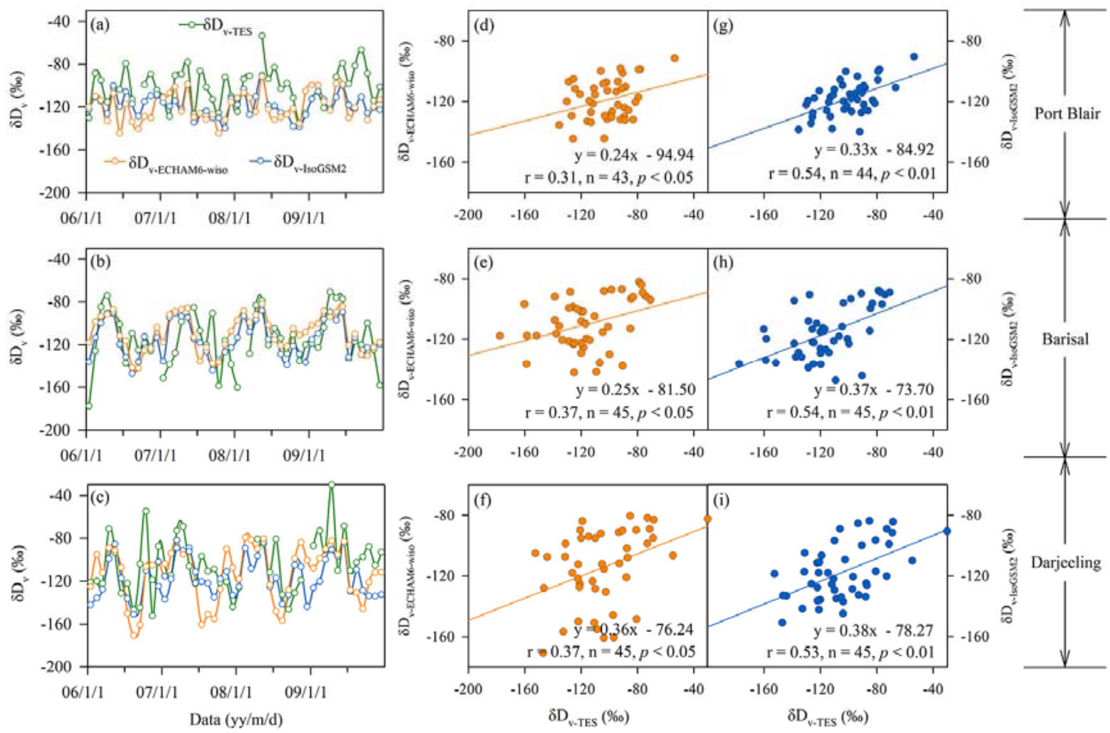

Figure S2. (a–c) Comparisons of monthly δD_v from TES (weighted by specific humidity over 1000–500 hPa) (green lines with dots) with modeled monthly δD_v from ECHAM6-wiso and IsoGSM2 (weighted by specific humidity over 1000–500 hPa) (orange and blue lines with dots, respectively) at Port Blair (a), Barisal (b), and Darjeeling (c). (d–f) The relationships between the monthly δD_v from TES and the ECHAM6-wiso modeled monthly δD_v at Port Blair (d), Barisal (e), and Darjeeling (f). (g–i) The same plots as (d–f) but for the relationships between the monthly δD_v from TES and the IsoGSM2 modeled monthly δD_v.

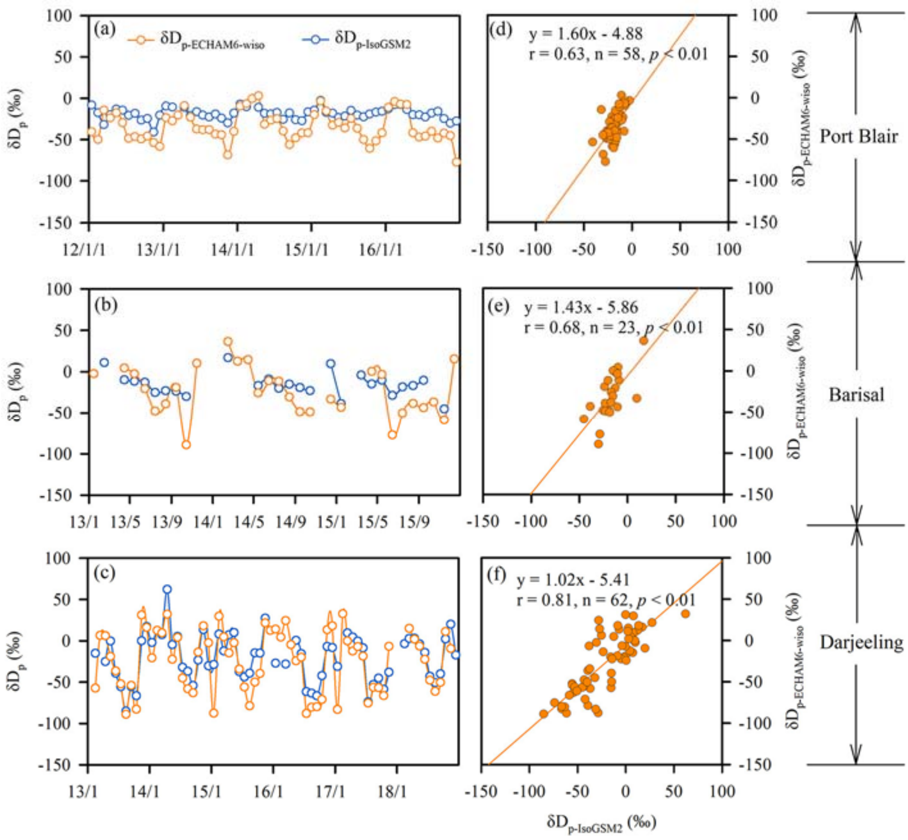

Figure S3. (a–c) Comparisons between the ECHAM6-wiso modeled δD_p and IsoGSM2 modeled δD_p at Port Blair (a), Barisal (b), and Darjeeling (c). (d–f) The relationships between the ECHAM6-wiso modeled δD_p and IsoGSM2 modeled δD_p at Port Blair (d), Barisal (e), and Darjeeling (f).

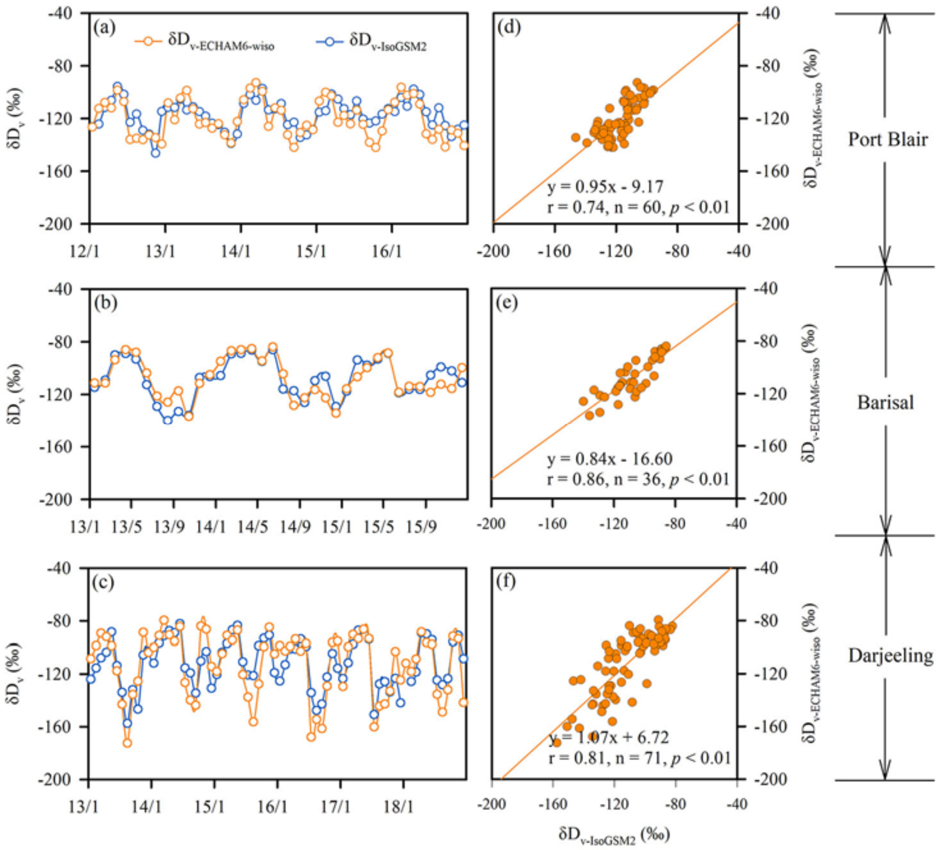

Figure S4. (a–c) Comparisons between the ECHAM6-wiso modeled δD_v and IsoGSM2 modeled δD_v at Port Blair (a), Barisal (b), and Darjeeling (c). (d–f) The relationships between the ECHAM6-wiso modeled δD_v and IsoGSM2 modeled δD_v at Port Blair (d), Barisal (e), and Darjeeling (f).

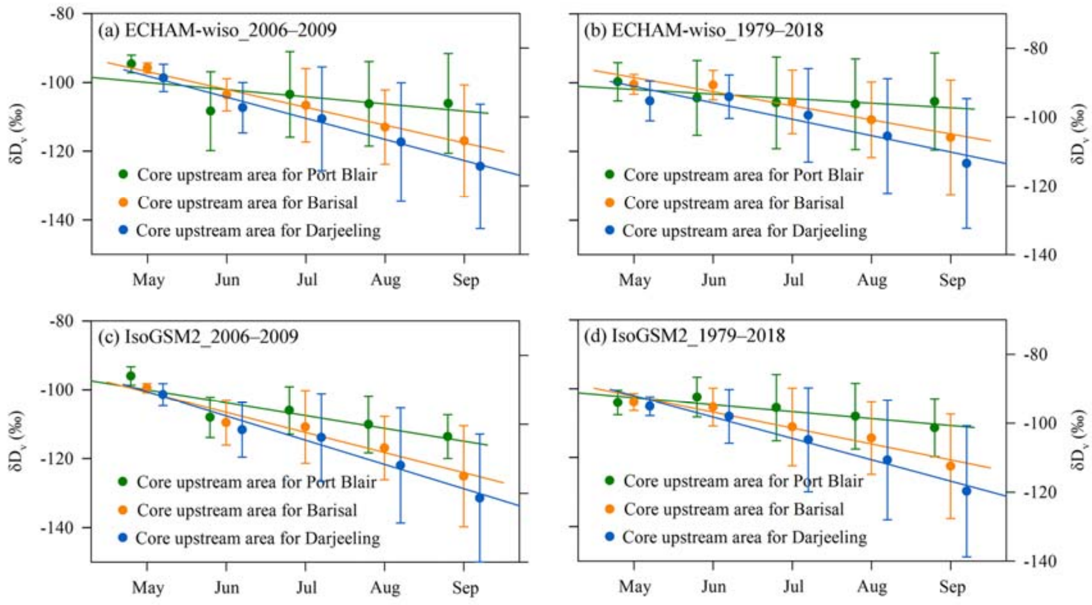

Figure S5. (a–b) Temporal variations of specific humidity weighted average δD_v over 1000–500 hPa in the core upstream areas for the three downstream study sites during 2006–2009 (a) and 1979-2018 (b) from ECHAM6-wiso. (c–d) Same as (a–b) but with the modeled δD_v from IsoGSM2.

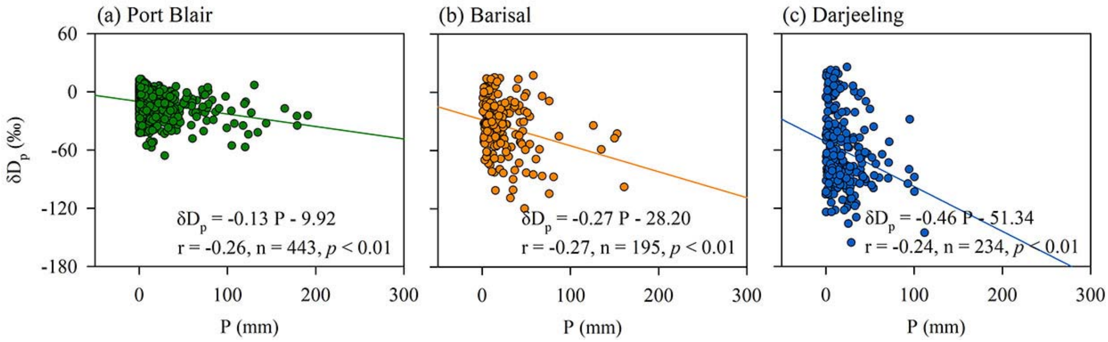

Figure S6. Relationships between the observed daily δD_p values and local precipitation amount (P) at Port Blair (a), Barisal (b), and Darjeeling (c).

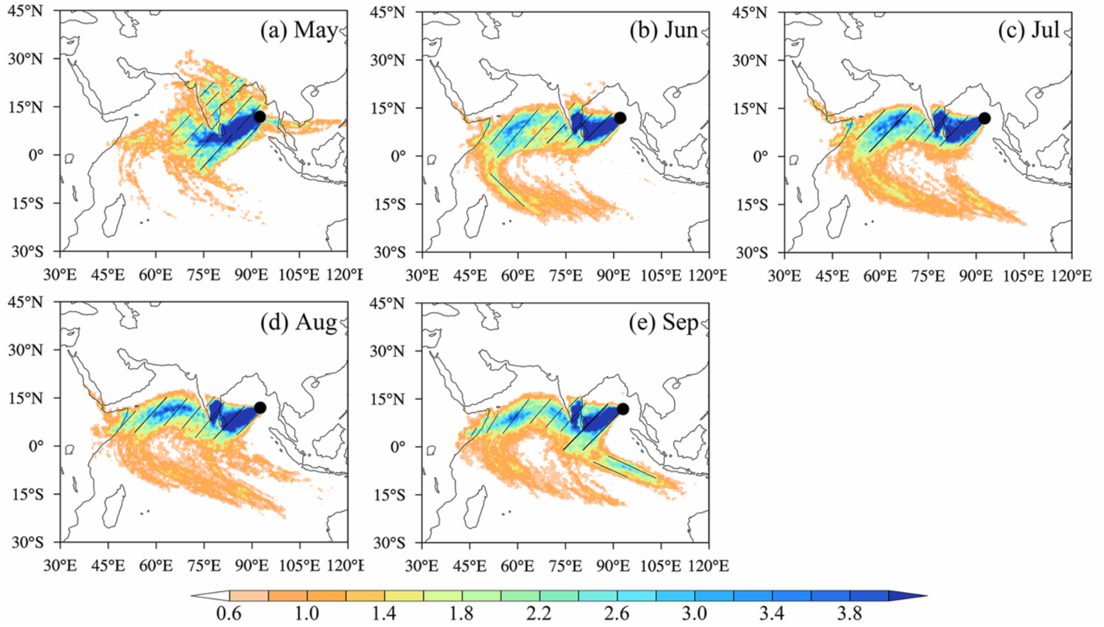

Figure S7. Spatial distributions of the multi-monthly mean fractional moisture contribution (10^{-4}) calculated by specific humidity parameter on back trajectories from ERA-Interim data for Port Blair (black dot) in May (a), June (b), July (c), August (d), and September (e). The diagonal lines mark the core upstream areas.

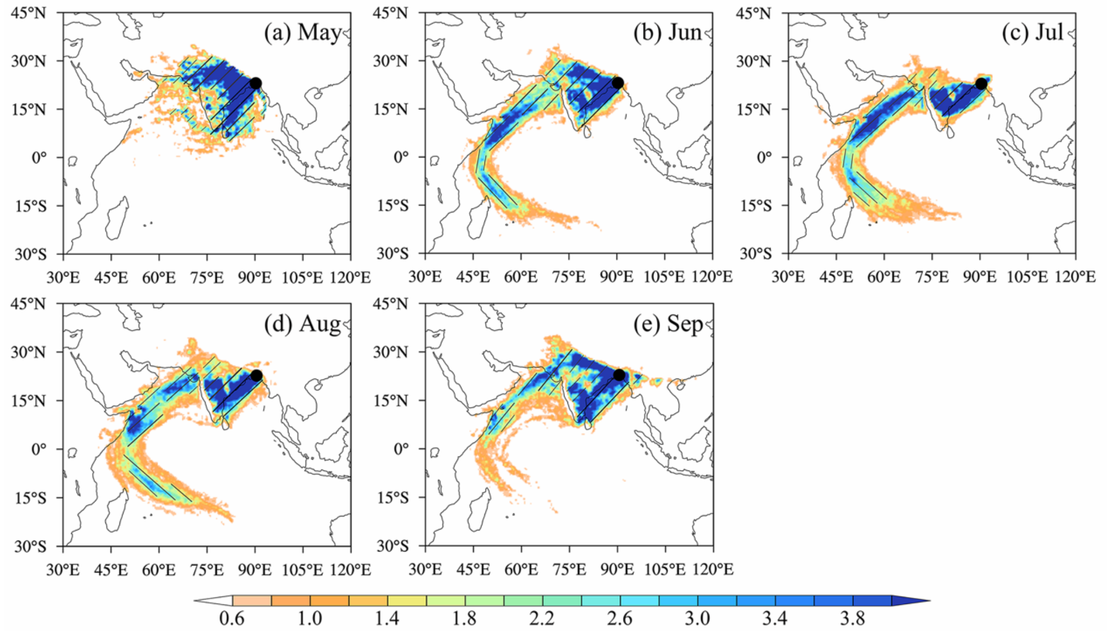

Figure S8. The same plots as shown in Fig. S7, but for Barisal (black dot). The diagonal lines mark the core upstream areas.

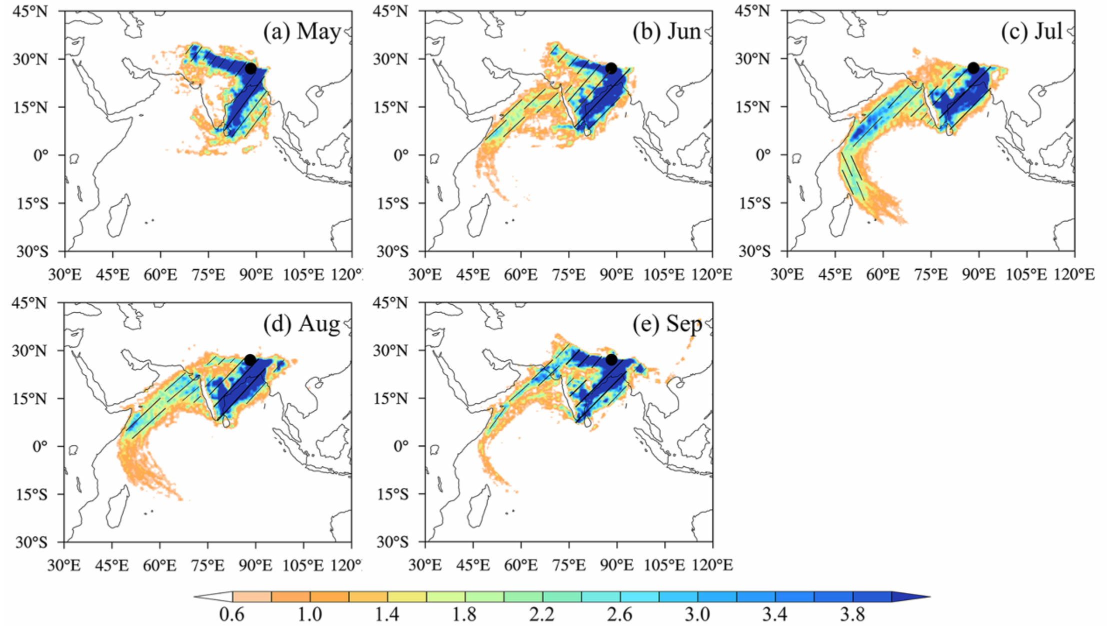

Figure S9. The same plots as shown in Fig. S7, but for Darjeeling (black dot). The diagonal lines mark the core upstream areas.

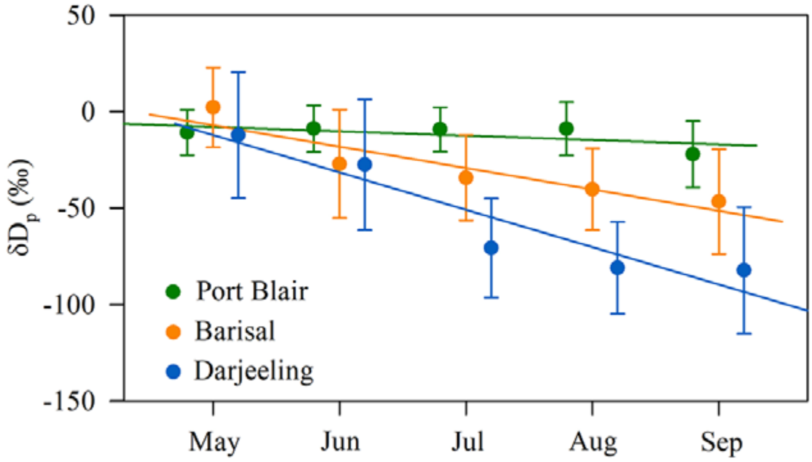

Figure S10. Temporal variations of the observed δD_p at the three downstream sites from May to September. The dots indicate the mean and standard deviations are marked by error bars.

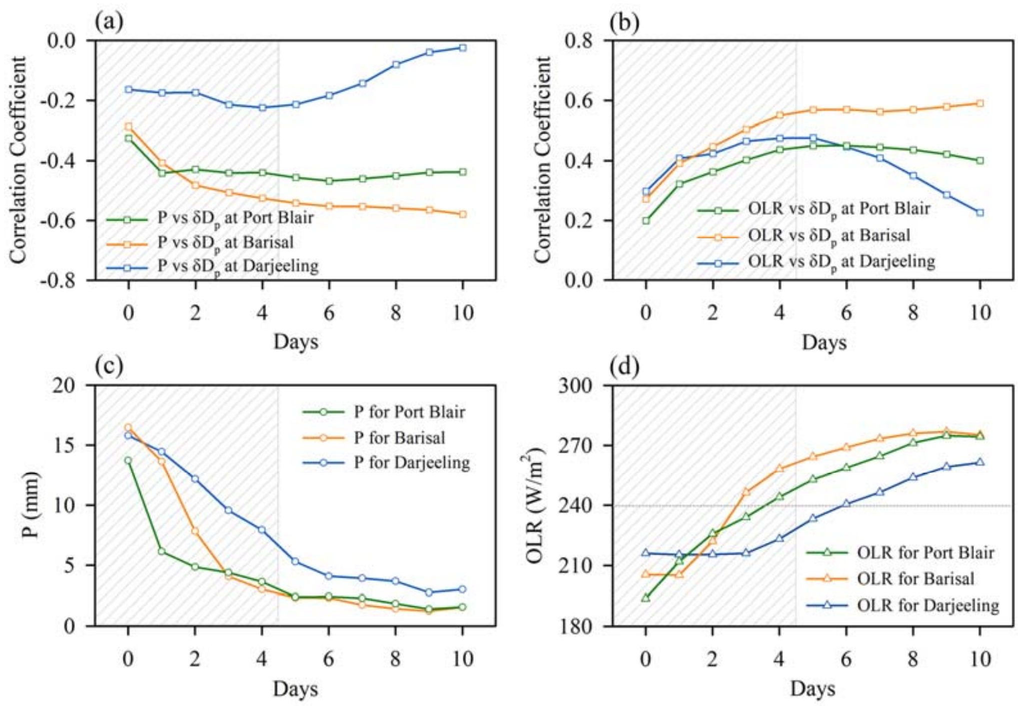

Figure S11. (a) Correlation coefficients between the observed daily δD_p at the three downstream study sites and the upstream accumulative P along the back trajectories over the time constant τ_m. (b) Correlation coefficients between the daily δD_p at the three downstream study sites and the upstream average OLR along the back trajectories over the time constant τ_m. Note that all the correlations are significant ($p <$ 0.01) except τ_m = 8–10 for Darjeeling in (a). (c) Changes in P along the back trajectories over the time constant τ_m for the three study sites. (d) The same plot as (c), but for OLR. The diagonal lines in (a–d) mark the range of 0–4 days. The horizontal dotted line in (d) marks the level where OLR is equal to 240 W/m^2.

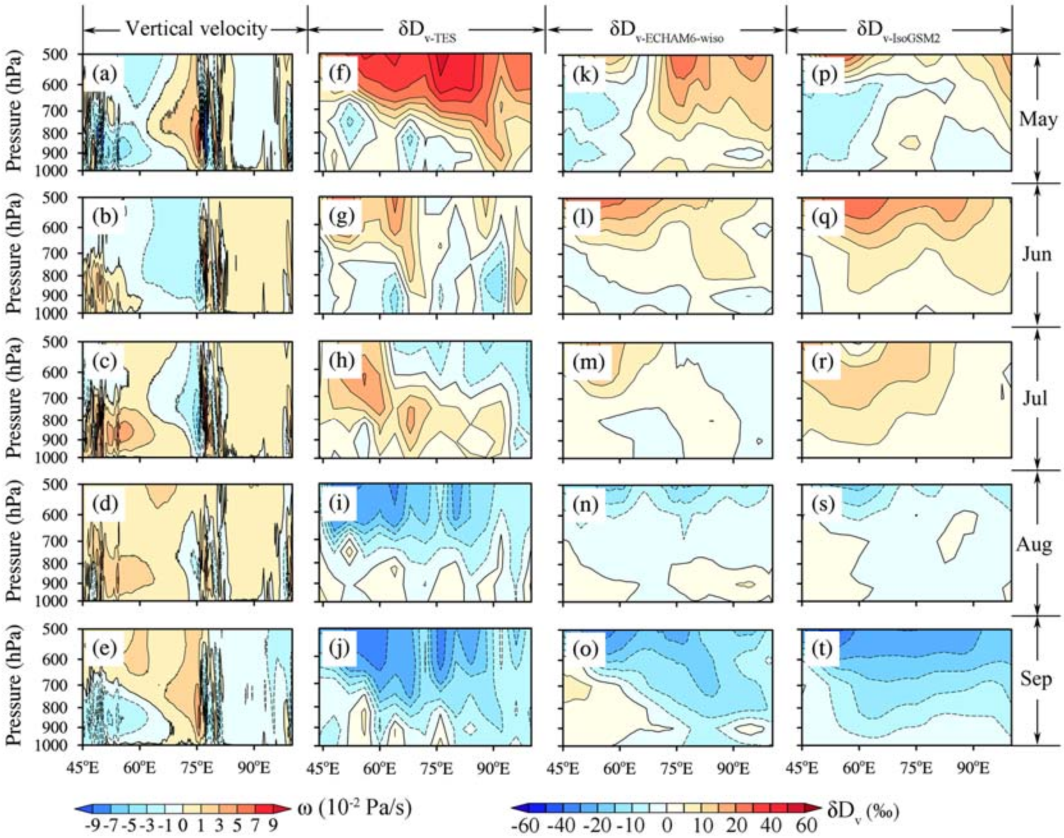

Figure S12. (a–e) Vertical profiles of meridional average (5–13°N) vertical velocity (ω) anomalies based on ERA5 reanalysis data across the upstream moisture contribution areas for Port Blair in May (a), June (b), July (c), August (d), and September (e). Negative anomaly values in (a–e) indicate upward motion, and positive anomaly values indicate downward motion. (f–j) Vertical profiles of meridional mean (5–13°N) δD_v anomalies from TES across the upstream moisture contribution areas for Port Blair in May (f), June (g), July (h), August (i), and September (j). (k–o) Same as (f–j) but with the δD_v values from ECHAM6-wiso. (p–t) Same as (f–j) but with the δD_v values from IsoGSM2.

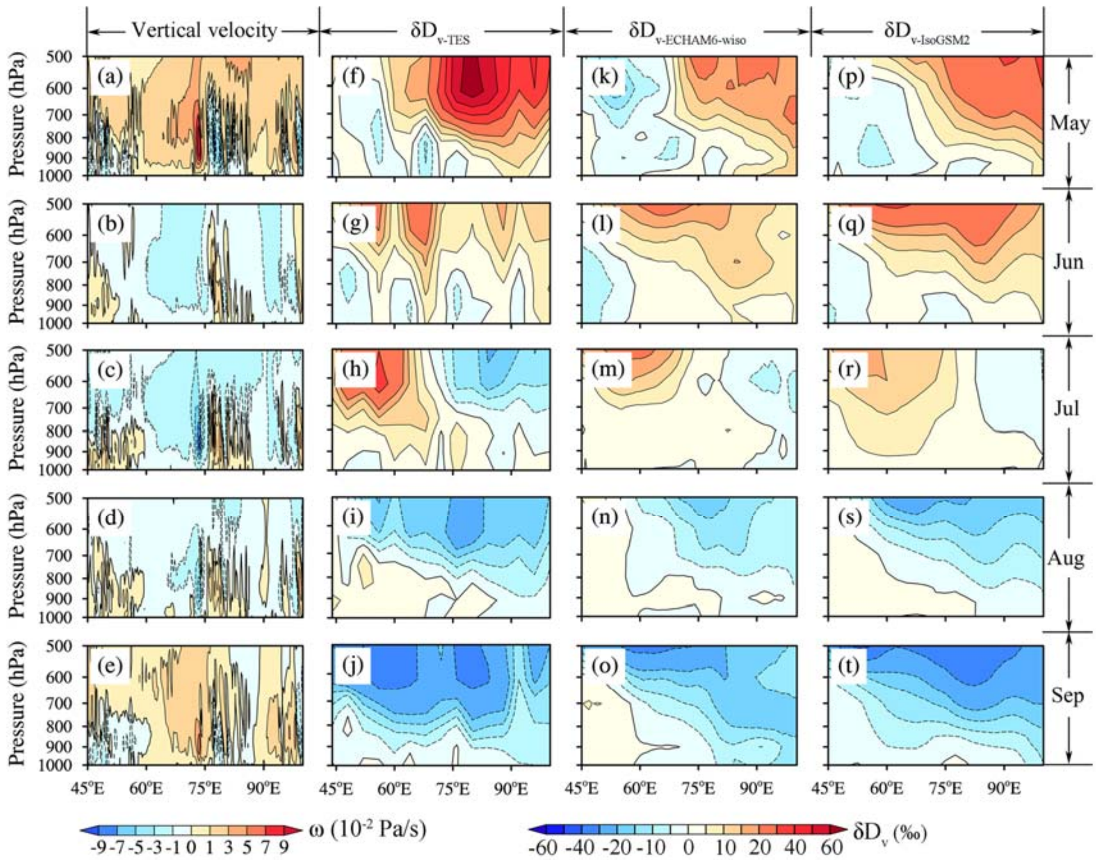

Figure S13. Same as Fig. S12 but with a meridional mean over the latitude band 5–26°N for Barisal.

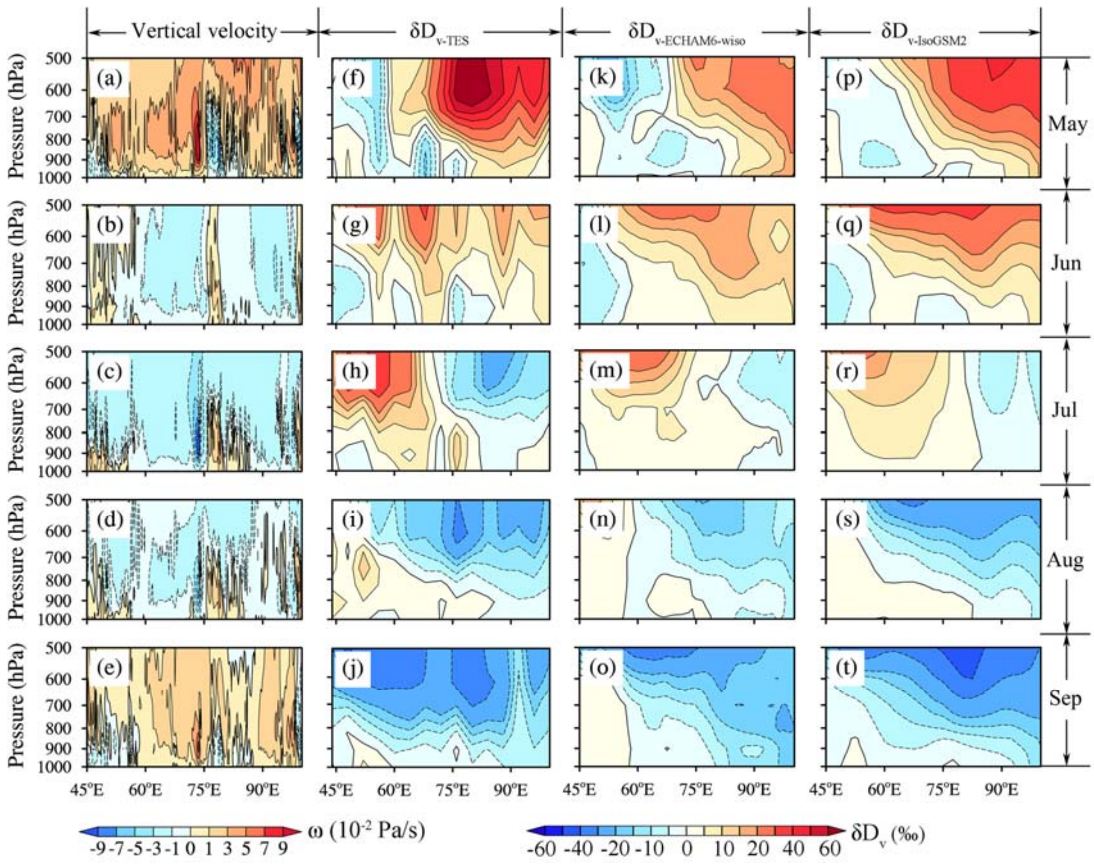

Figure S14. Same as Fig. S12 but with a meridional mean over the latitude band 10–28°N for Darjeeling.

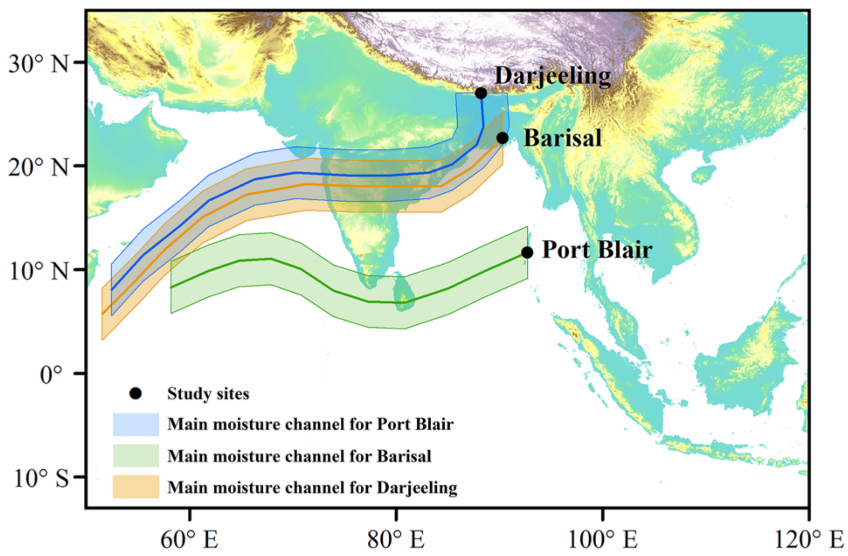

Figure S15. Main moisture channels during May–September for Port Blair, Barisal, and Darjeeling.

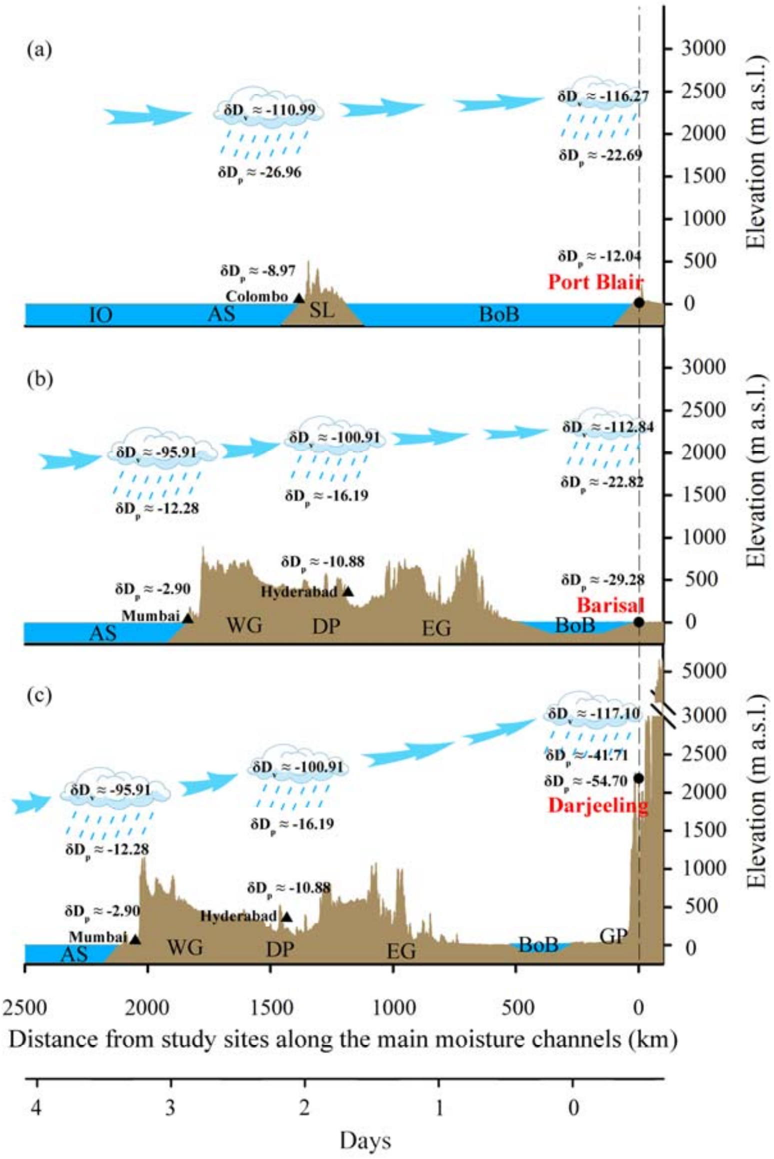

Figure S16. Same as Figure 4 but with the modeled δD_v and δD_p values from IsoGSM2.